

Chapter 2

Methodology

This chapter describes the methods that are used in this study. Prior to the methodology, the notation used in this chapter is explained in section 2.0. Section 2.1 introduces the shallow water model whose simulations are used throughout this study. Energetics in the shallow water model and the formulation of the backscatter parametrization are succeedingly discussed in section 2.1.4. The analysis of Reynolds and Rossby numbers is based on definitions provided in section 2.2. In section 2.3, details on the computation of the eddy kinetic energy spectrum are given. The analysis of Lagrangian trajectories is presented in section 2.4 and finally a short remark on the data sampling from the shallow water model is provided in section 2.5.

2.0 Notation

In the following, we will make use of a notation, where

- (i) a scalar variable a, A is written in normal font with either lower or upper case letter. A vector $\mathbf{a} = (a_1, a_2)$ is written in bold-font but lower case. A tensor $\mathbf{A} = (A_1, A_2; A_3, A_4)$ is written with upper case bold letters.
- (ii) the product \cdot between a vector $\mathbf{a} = a_i$ and a tensor $\mathbf{C} = C_{ij}$ is defined as $\mathbf{a} \cdot \mathbf{C} = \sum_i a_i C_{ij} = d_j$ and yields a vector $d_j = \mathbf{d}$.
- (iii) two vectors $\mathbf{a} = (a_1, a_2)$, $\mathbf{b} = (b_1, b_2)$ concatenated without any symbol, i.e. \mathbf{ab} , yield a tensor \mathbf{C} , such that $\mathbf{ab} = (a_1b_1, a_1b_2; a_2b_1, a_2b_2) = \mathbf{C}$.
Example given: $\nabla \mathbf{u} = (\partial_x u, \partial_x v; \partial_y u, \partial_y v)$
- (iv) the 2-norm of a vector $\mathbf{a} = (a_1, a_2)$ is written as $|\mathbf{a}| = \sqrt{a_1^2 + a_2^2}$. Similarly the 2-norm of the tensor \mathbf{A} is $|\mathbf{A}| = \sqrt{A_1^2 + A_2^2 + A_3^2 + A_4^2}$. For a complex number $z = a + ib$, $|z| = \sqrt{a^2 + b^2}$.

2.1 The shallow water model

The shallow water model follows from the depth-integrated Navier-Stokes equations with the assumption that the vertical length scale is negligible compared to the horizontal length scale [Gill, 1982; Vallis, 2006]. In this study we use the shallow water equations of the form

$$\partial_t u + u\partial_x u + v\partial_y u - fv = -g\partial_x \eta + F_x + B_x + M_x + \xi_x \quad (2.1a)$$

$$\partial_t v + u\partial_x v + v\partial_y v + fu = -g\partial_y \eta + F_y + B_y + M_y + \xi_y \quad (2.1b)$$

$$\partial_t \eta + \partial_x(uh) + \partial_y(vh) = 0 \quad (2.1c)$$

with

$\mathbf{u} = (u, v) = (u(x, y, t), v(x, y, t))$	horizontal velocity vector
$\eta = \eta(x, y, t)$	surface displacement
$h = h(x, y, t) = \eta + H$	layer thickness
$H = \text{constant}$	undisturbed layer thickness
$f = f(y)$	Coriolis parameter
$g = \text{constant}$	gravitational acceleration
$\mathbf{f} = (F_x, F_y) = (F_x(x, y, t), F_y(x, y, t))$	forcing vector
$\mathbf{b} = (B_x, B_y) = (B_x(u, v, h), B_y(u, v, h))$	bottom friction term
$\mathbf{m} = (M_x, M_y) = (M_x(u, v, h), M_y(u, v, h))$	lateral mixing of momentum
$\Xi = (\xi_x, \xi_y)$	negative viscosity backscatter

and differential operators $\partial_x = \frac{\partial}{\partial x}$, $\partial_y = \frac{\partial}{\partial y}$, $\partial_t = \frac{\partial}{\partial t}$ on the rectangular domain $\mathcal{D} = (0, L_x) \times (0, L_y)$ of width (or east-west extent) L_x and north-south extent L_y and with cartesian coordinates x, y and time t . As initial conditions we choose to start from rest, so that $u = v = \eta = 0$ at $t = 0$. There is no flow through the boundary, which is usually referred to as the kinematic boundary condition (equation A.1). We set the tangential velocity at the boundary to zero in order to have no-slip boundary conditions (equation A.3). This is motivated as free-slip boundary conditions (equation A.4) in contrast yield an enormous western boundary current that is maintained by eddies propagating via the northern boundary towards the east. In order to

have some resemblance of the shallow water model with the circulation in mid-latitudinal ocean basins, we favour no-slip boundary conditions.

In the following, the formulation of the terms appearing in the shallow water equations 2.1 are presented. A detailed description about the discretization of the shallow water equations 2.1 is found in appendix A.2. It is based on an equivalent formulation of the shallow water equations as presented in appendix A.1.2.

2.1.1 Barotropic double gyre wind forcing

In order to simulate mid-latitudinal dynamics, we choose the physical parameters of the previous section as [Berloff, 2005; Cooper & Zanna, 2015; Porta Mana & Zanna, 2014; Zanna *et al.*, 2017]

$$g = 10 \text{ ms}^{-2}, \quad H = 500 \text{ m}, \quad L_x = L_y = 3840 \text{ km} \quad (2.2)$$

with beta-plane approximation [Gill, 1982]

$$f = f_0 + \beta(y - \frac{L_y}{2}), \quad f_0 = 2\Omega \sin(2\pi \frac{\theta_0}{360}), \quad \beta = \frac{2\Omega}{R} \cos(2\pi \frac{\theta_0}{360}) \quad (2.3)$$

at northern hemisphere mid-latitudes, with the domain \mathcal{D} being centred around the latitude $\theta_0 = 30$ with

$$R = 6371 \text{ km}, \quad \Omega = \frac{2\pi}{86400} \text{ s}^{-1}. \quad (2.4)$$

The forcing is set to be $F_y = 0$ and

$$F_x = \frac{\gamma}{\rho h} \quad (2.5a)$$

$$\gamma = F_0 \left[\cos \left(2\pi \left(\frac{y}{L_y} - \frac{1}{2} \right) \right) + 2 \sin \left(2\pi \left(\frac{y}{L_y} - \frac{1}{2} \right) \right) \right] \quad (2.5b)$$

with amplitude $F_0 = 0.12 \text{ Pa}$ and density $\rho = 1000 \text{ kgm}^{-3}$. The forcing F_x resembles the trade winds in the southern part of the domain and the westerlies in the northern part of the domain (Fig. 2.1). We admit that the choice of H yields an unrealistically shallow ocean basin. The wind forcing is increased by a factor of three compared to reference values [Cooper & Zanna, 2015]. However, we thereby increase the allowed numerical time step (see section A.2.9) leading to a reduced effective computing time for a more

turbulent shallow water system.

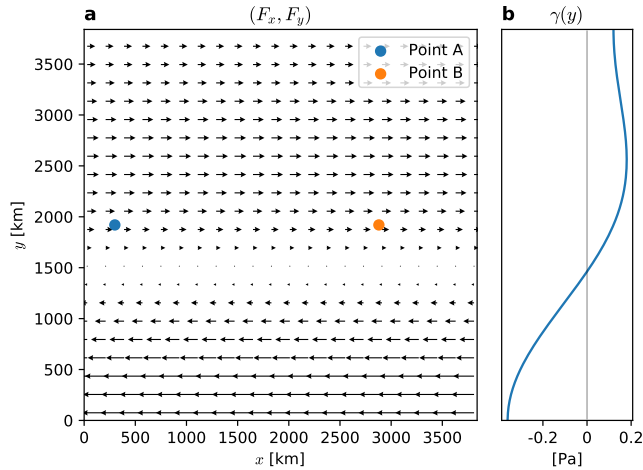


Figure 2.1: (a) The wind forcing (F_x, F_y) resembling trade winds and westerlies over the domain \mathcal{D} . (b) Wind profile γ . The points A, B will be used for the analysis of autocorrelation (section 3.6, Fig. 3.10 and 3.11).

2.1.2 Bottom friction

A quadratic drag of the following form is used for all model runs with bottom friction

$$\mathbf{b} = -\frac{c_D}{h} |\mathbf{u}| \mathbf{u} \quad (2.6)$$

with c_D being a dimensionless drag coefficient [Arbic & Scott, 2008]. In contrast to a linear drag, a quadratic drag was found to be more realistic. It removes energy especially at the larger scales, leaving the smaller scales almost unaffected. This is supported in this study (see section 3.4).

The energetics of the bottom friction term are presented in section 2.1.4. In this study, we investigate a set of model runs containing bottom friction where we choose $c_D = 10^{-5}$ and another set of model runs without bottom friction ($c_D = 0$) as described in Table 2.1. The choice of c_D is discussed in section A.2.6.

2.1.3 Lateral mixing of momentum

The viscosity is formulated as lateral mixing of momentum and represented by the term \mathbf{m} . A general approach \mathbf{m}_0 of this family being

$$\mathbf{m}_0 = \nabla \cdot \nu \mathbf{S} \quad (2.7)$$

with the viscosity coefficient ν and a stress tensor \mathbf{S} (sometimes also called viscous flux tensor [Eden, 2016]). With $\mathbf{S} = \nabla \mathbf{u}$ and a constant ν the equation 2.7 reduces to

$$\mathbf{m}_L = \nu \nabla^2 \mathbf{u} \quad (2.8)$$

with $\nabla^2 = \partial_x^2 + \partial_y^2$ the two dimensional Laplace operator. However, as discussed by Shchepetkin & O'Brien [1996] a more sophisticated alternative is found with the symmetric 2x2 stress tensor \mathbf{S} defined by

$$\mathbf{S} = \begin{pmatrix} u_x - v_y & v_x + u_y \\ v_x + u_y & -(u_x - v_y) \end{pmatrix}. \quad (2.9)$$

Their harmonic lateral mixing of momentum term \mathbf{m}_2 is then formulated for the shallow water model as

$$\mathbf{m}_2 = \nu_A h^{-1} \nabla \cdot h \mathbf{S}. \quad (2.10)$$

Note that for h being a constant equation 2.10 simplifies to equation 2.8. Equation 2.10 can be extended to a biharmonic operator by applying it twice

$$\mathbf{m} = \nu_B h^{-1} \nabla \cdot (h \mathbf{S}(h^{-1} \nabla \cdot h \mathbf{S}(u, v))). \quad (2.11)$$

where the stress tensor is regarded as a linear map, once evaluated with (u, v) and then with $h^{-1} \nabla \cdot h \mathbf{S}(u, v)$. Both viscosity coefficients ν_A and ν_B are for simplicity taken as constants. Again, for a constant h equation 2.11 reduces to $\nu_B \nabla^4 \mathbf{u}$, with $\nabla^4 = \partial_x^4 + \partial_y^4 + 2\partial_x^2 \partial_y^2$. Hence, for a barotropic system, where $\eta \ll H$ it might be justified to linearize the viscous term by assuming h to be constant as in Cooper & Zanna [2015]. However, here we keep the form of equation 2.11 to have a fully non-linear system. A higher order derivative implies the use of higher order boundary conditions: Applying the harmonic

operator twice yields additional boundary conditions as

$$h\nabla^2 u + \nabla h \cdot \begin{pmatrix} u_x - v_y \\ v_x + u_y \end{pmatrix} = 0, \quad \text{at } x = 0 \quad \text{and} \quad x = L_x \quad (2.12)$$

and

$$h\nabla^2 v + \nabla h \cdot \begin{pmatrix} v_x + u_y \\ v_y - u_x \end{pmatrix} = 0, \quad \text{at } y = 0 \quad \text{and} \quad y = L_y \quad (2.13)$$

For the case of a constant h this simplifies to a vanishing second derivative of the normal velocity component at the boundaries.

A biharmonic operator acts especially on the small scales, where waves are rapidly damped compared to the large scales, which remain mostly unaffected [Griffies & Hallberg, 2000; Shchepetkin & O'Brien, 1996]. To have an additional energy sink at the large scales, bottom friction from equation 2.6 is used in combination with the biharmonic lateral mixing of momentum as presented here. For a discussion on the choice of ν_B the reader is referred to section A.2.6. The choices for the different model runs are listed in Table 2.1.

2.1.4 Energetics in the shallow water model

In the following, energy sources/sinks and reservoirs in the shallow water system are discussed as they will be analyzed for all model runs in section 3.4.

The shallow water equations without forcing or dissipation (i.e. $\mathbf{f} = \mathbf{m} = \mathbf{b} = 0$) obey a conservation of energy of the form

$$\partial_t \langle \frac{1}{2} \rho h (u^2 + v^2) + \frac{1}{2} g \rho \eta^2 \rangle = 0. \quad (2.14)$$

For a detailed derivation see Appendix A.3.1. The first term represents kinetic energy KE and the second (available) potential energy PE, both horizontally integrated by $\langle \rangle = \int \int_{\mathcal{D}} \mathrm{d}\mathbf{x}$ and vertically as are the momentum equations (2.1).

Energetics of wind forcing Once we consider wind forcing F_x in equation 2.1a of the form as in equation 2.5

$$\partial_t u = \dots + \frac{\gamma}{\rho h} \quad (2.15)$$

the energy $\langle \text{KE} + \text{PE} \rangle$ is not conserved

$$\partial_t \langle \text{KE} + \text{PE} \rangle = \langle u \gamma \rangle \quad (2.16)$$

Once u and F_x are of the same sign, i.e. the flow follows the direction of the wind, the wind forcing term is a source of energy to the shallow water system. As we start the model runs from rest we can expect at least in the sense of a spatial and temporal average that the wind forcing is a source of energy to the shallow water system. This is discussed and supported in section 3.4.

Energetics of bottom friction Consider adding a drag term of the form in equation 2.6

$$\partial_t \mathbf{u} = \dots - \frac{c_D}{h} \sqrt{u^2 + v^2} \mathbf{u} \quad (2.17)$$

that acts physically as bottom friction. The energy equation is then

$$\partial_t \langle \text{KE} + \text{PE} \rangle = -\langle \rho c_D (u^2 + v^2)^{\frac{3}{2}} \rangle \leq 0. \quad (2.18)$$

which is with non-vanishing velocities an energy sink throughout the domain \mathcal{D} at every time step.

Energetics of lateral mixing A term of the form

$$\partial_t \mathbf{u} = \dots + h^{-1} \nabla \cdot (\nu h \mathbf{S}) \quad (2.19)$$

with viscosity coefficient $\nu > 0$ and stress tensor \mathbf{S} is added to the momentum equations. In fact, using a biharmonic lateral mixing of momentum this term should be negative to account for the correct sign of diffusion. Adaptation of the following for a biharmonic operator is straight forward. The energy equation is then

$$\partial_t \langle \text{KE} + \text{PE} \rangle = \langle \rho \mathbf{u} \cdot (\nabla \cdot \nu h \mathbf{S}) \rangle. \quad (2.20)$$

By evaluating

$$\mathbf{u} \cdot (\nabla \cdot \nu h \mathbf{S}) = \nabla \cdot (\nu h \mathbf{S} \cdot \mathbf{u}) - \nabla \mathbf{u} \cdot \nu h \mathbf{S} \quad (2.21)$$

and making use of the kinematic boundary condition the first term vanishes in the global integral as divergence of a flux and it follows that

$$\partial_t \langle \text{KE} + \text{PE} \rangle = -\langle \rho \nu h \nabla \mathbf{u} \cdot \mathbf{S} \rangle. \quad (2.22)$$

For the case of \mathbf{S} being the symmetric stress tensor defined in equation 2.9, i.e. harmonic diffusion, lateral mixing is an energy sink as $\partial_t \langle \text{KE} + \text{PE} \rangle = -\langle \rho \nu h \nabla \mathbf{u} \cdot \mathbf{S} \rangle \leq 0$ not just spatially integrated but everywhere in the domain \mathcal{D} (see section A.3.3 for details). This is in contrast to biharmonic mixing operators (equation 2.11), which are not sign-definite in that respect. As a result, the harmonic diffusion is always down-gradient, but the biharmonic diffusion can also lead to local power input in equation 2.22 [Griffies, 2004], but is in general also an energy sink.

Mean and eddy kinetic and potential energy Using Reynolds - decomposition in time allows to split every quantity a into a time mean \bar{a} and anomalies a' relative to \bar{a} as

$$a = \bar{a} + a'. \quad (2.23)$$

However, in the shallow water system it is proposed to use thickness-weighted averaging [Aiki *et al.*, 2016]

$$\hat{a} = \frac{\overline{ha}}{\bar{h}} \quad (2.24)$$

The thickness-weighted average \hat{a} is then used to compute the respective anomalies a''

$$a'' = a - \hat{a} \quad (2.25)$$

Note that $\overline{ha''} = 0$. We can split the potential energy PE into mean potential energy (MPE) and eddy potential energy (EPE) with the thickness-unweighted decomposition

$$\overline{\text{PE}} = \overline{\frac{1}{2}g\rho(\bar{\eta} + \eta')^2} = \frac{1}{2}g\rho\bar{\eta}^2 + \frac{1}{2}g\rho\overline{\eta'^2} \equiv \text{MPE} + \text{EPE}. \quad (2.26)$$

For mean kinetic energy (MKE) and eddy kinetic energy (EKE) we use thickness-weighted decomposition on u and v

$$\begin{aligned}
 \overline{\text{KE}} &= \overline{\frac{1}{2}\rho h ((\widehat{u} + u'')^2 + (\widehat{v} + v'')^2)} \\
 &= \frac{1}{2}\rho \left(\overline{h(\widehat{u}^2 + \widehat{v}^2)} + \overline{h(u''^2 + v''^2)} + 2\overline{\widehat{u}hu''} + 2\overline{\widehat{v}hv''} \right) \\
 &= \frac{1}{2}\rho \overline{h(\widehat{u}^2 + \widehat{v}^2)} + \frac{1}{2}\rho \overline{h(u''^2 + v''^2)} \\
 &\equiv \text{MKE} + \text{EKE}
 \end{aligned} \tag{2.27}$$

2.2 Reynolds and Rossby numbers

Definitons of the Reynolds and Rossby numbers directly calculated from the size of terms in the shallow water equations and adapted to the energy budget-based backscatter parametrization are presented.

Reynolds number The Reynolds number, defined as the ratio between advective and viscous terms, is traditionally estimated via scale analysis

$$\widehat{R}_e = \frac{\mathcal{O}((\mathbf{u} \cdot \nabla)\mathbf{u})}{\mathcal{O}(\nu \nabla^2 \mathbf{u})} = \frac{UL}{\nu} \tag{2.28}$$

with some velocity scale U , length scale L and viscosity ν . It is also possible to directly compute the size of the advective and viscous term, i.e. replacing the $\mathcal{O}()$ -operation by the 2-norm of a vector and using the lateral mixing of momentum from equation (2.11)

$$R_e = \frac{|(\mathbf{u} \cdot \nabla)\mathbf{u}|}{|\nu_B h^{-1} \nabla \cdot (h\mathbf{S}(h^{-1} \nabla \cdot h\mathbf{S}(u, v)))|} \tag{2.29}$$

In the case of the backscatter parametrization, the effective Reynolds number R_e^* also includes the backscatter term

$$R_e^* = \frac{|(\mathbf{u} \cdot \nabla)\mathbf{u}|}{|\nu_B h^{-1} \nabla \cdot (h\mathbf{S}(h^{-1} \nabla \cdot h\mathbf{S}(u, v))) + \nu_{\text{back}} h^{-1} \nabla \cdot h\mathbf{S}|} \tag{2.30}$$

in order to account for the negative viscosity introduced by the backscatter parametrization. In fact, the terms in the denominator counteract each other: The first tends to smooth gradients, whereas the second tends to steepen them. Using the backscatter parametrization we can expect that $R_e^* > R_e$ in an average sense.

Rossby number Via scale analysis the Rossby number \widehat{R}_o results from the ratio of advective terms and Coriolis terms as

$$\widehat{R}_o = \frac{\mathcal{O}((\mathbf{u} \cdot \nabla)\mathbf{u})}{\mathcal{O}(f\mathbf{k} \times \mathbf{u})} = \frac{U}{fL} \quad (2.31)$$

with f being the Coriolis parameter and \mathbf{k} the unity vector in the vertical. As in equation (2.29) the direct calculation for the Rossby number R_o yields

$$R_o = \frac{|(\mathbf{u} \cdot \nabla)\mathbf{u}|}{|f\mathbf{k} \times \mathbf{u}|}. \quad (2.32)$$

It is also possible to base an estimation R_o^* of the Rossby number on the deformation rate

$$|D| = \sqrt{(\partial_x u - \partial_y v)^2 + (\partial_y u + \partial_x v)^2} \quad (2.33)$$

which yields a large Rossby number R_o^* in regions with strong shear flow

$$R_o^* = \frac{|D|}{f} \quad (2.34)$$

Histogram computation The direct Reynolds numbers R_e and Rossby numbers R_o will be investigated in terms of their histogram computed for all grid cells and all available time steps (without the spin-up phase, see section 2.5) at daily resolution. Hence, the histograms are computed from roughly $1.5 \cdot 10^8$ values in the low resolution case and $2.4 \cdot 10^9$ at high resolution. The high resolution histograms are divided by a factor 16 to account for this and allow normalization onto the low resolution histograms. As Rossby and Reynolds numbers are approximately log-normally distributed the histogram is computed over their respective logarithms with a bin width of about 0.027 for Reynolds numbers and 0.018 for Rossby numbers. Also, a spatio-temporal mean Rossby and Reynolds number is computed, where the logarithm is applied afterwards for visualization purposes. For the model runs including backscatter, the effective Reynolds number R_e^* is used instead to account for the backscatter term.

Rossby radius of deformation The Rossby radius of deformation L_{R_o} is defined via the shallow water phase speed for gravity waves $c_{ph} = \sqrt{gH}$ (see discussion around equation A.75 for further details) and the Coriolis

parameter $f = f(y)$ as

$$L_{Ro} = \frac{c_{ph}}{f}. \quad (2.35)$$

In the beta-plane approximation (equation 2.3), the Rossby radius is largest at the southern edge of the domain ($y = 0$) and smallest at the northern edge ($y = L_y$), it is therefore further distinguished between

$$L_{Ro}^{\max} = \frac{c_{ph}}{f_0 - \beta \frac{L_y}{2}} \quad \text{and} \quad L_{Ro}^{\min} = \frac{c_{ph}}{f_0 + \beta \frac{L_y}{2}}. \quad (2.36)$$

2.3 Eddy kinetic energy spectrum

To have an objective analysis about the effect of sub-grid scale parametrizations, the eddy kinetic energy spectrum $\text{EKE}(K)$ as a function of the total wavenumber $K = \sqrt{k^2 + l^2}$ is regarded. k is the zonal wavenumber (in x -direction), l the meridional wavenumber (in y -direction). Such a spectrum is especially sensitive to oscillations that may appear at the grid scale once dissipation is too weak. In this case, kinetic energy tends to pile up at the largest wave numbers, which results from the numerics and is physically undesired. The spectrum is defined as [Jansen *et al.*, 2015]

$$\text{EKE}(K) = \frac{d}{dK} \iint_{k^2 + l^2 < K^2} \frac{1}{2} \left(|\widehat{u}_t|^2 + |\widehat{v}_t|^2 \right) dkdl \quad (2.37)$$

with $\widehat{u}_t, \widehat{v}_t$ being the spectral transforms of the two dimensional fields u, v for a given time t . The overbar denotes a temporal mean. The EKE spectrum regarded here therefore describes the energy per wavenumber (regardless of the direction) averaged in spectral space over all available time steps.

2.4 Lagrangian trajectories

To calculate the trajectory of a Lagrangian float, we follow the idea that at a given time t the position $\mathbf{x}_p = (x_p, y_p)$ of that particle changes by passive advection of the flow field

$$\frac{dx_p}{dt} = u(\mathbf{x} = \mathbf{x}_p), \quad \frac{dy_p}{dt} = v(\mathbf{x} = \mathbf{x}_p). \quad (2.38)$$

Providing the initial position of the float $\mathbf{x}_p(t = 0)$ we can solve equation 2.38 numerically with a given flow field (u, v) . As the flow field is gridded on the native model grid, which in general does not correspond to the float positions, we interpolate bilinearly from the four surrounding grid points. Taking the boundary conditions of the flow field into account, no float was observed to leave the domain \mathcal{D} . However, due to a vanishing flow some floats remain at the boundary for a long time, which is thought of to be physically reasonable.

Discretizing the time derivative in equation 2.38 is done with a predictor-corrector method (also known as trapezoidal rule, [Butcher, 2008]). With x_0, y_0 the initial positions at time $t = t_0$ and x_1, y_1 the positions at time $t = t_0 + \delta t$ this is

$$x_1 = x_0 + \frac{\delta t}{2}(u_0 + u_1), \quad y_1 = y_0 + \frac{\delta t}{2}(v_0 + v_1) \quad (2.39)$$

where $u_0 = u(t = t_0, \mathbf{x} = \mathbf{x}_0)$ and $v_0 = v(t = t_0, \mathbf{x} = \mathbf{x}_0)$ and $u_1 = u(t = t_0 + \delta t, \mathbf{x} = \mathbf{x}_1^*)$ and $v_1 = v(t = t_0 + \delta t, \mathbf{x} = \mathbf{x}_1^*)$ with the initial guess positions

$$x_1^* = x_0 + \delta t u_0, \quad y_1^* = y_0 + \delta t v_0 \quad (2.40)$$

that are computed with Euler forward. The float trajectories are calculated offline, hence the time step δt is 6 hours, as this is the smallest time step at which data from the numerical model is stored. We calculate trajectories from a total 100,000 floats, that were injected at 1000 random starting dates (after the spin-up phase) in groups of 100 floats. The trajectories are then calculated forward in time for one year. The results are presented in terms of *accumulated float density*, which accounts for all floats that have been at the respective location at some time within one year after release. That means, accumulated float density is a histogram that counts all floats that have been in a given grid box (equal boxes of $\Delta x = \Delta y = 15\text{km}$ are used), regardless of when they have been there within one year after release. The zero-isoline of that histogram therefore denotes the line that no float was able to cross within one year. As release locations, we pick for every float a random position within a rectangle that spans from $x = 100\text{km}$ to $x = 200\text{km}$ and from $y = 100\text{km}$ to $y = 1920\text{km}$ as marked in Fig. 3.12 to place the floats close to the boundary within the subtropical gyre (a discussion is given in section 3.7). If all floats were always far away from the boundary, then the

2. METHODOLOGY

accumulated float density would be calculated from in total 146,000,000 float positions (100,000 floats at 1460 time steps that result from 6-hourly data for 365 days). However, as some floats stay for a long time close to the boundary, as discussed above, these are neglected from analysis by disregarding all float positions that are closer than 30km to the boundary. In practice, this means that 98% of all theoretical positions enter the analysis for the control runs and 94% for the model runs with backscatter.

2.5 Model runs and data sampling

For the list of model runs that are analysed in this study see Table 2.1.

List of model runs	c_D	N_x	Δx [km]	ν_B [m ⁴ s ⁻¹]	n_{diss}	t_c
with bottom friction						
Low resolution (LR)	10^{-5}	128^2	30	$4.86 \cdot 10^{11}$	-	1
High resolution (HR)	10^{-5}	512^2	7.5	$7.59 \cdot 10^9$	-	50.2
LR + weak backscatter	10^{-5}	128^2	30	$4.86 \cdot 10^{11}$	$\frac{1}{2}$	1.39
LR + moderate backscatter	10^{-5}	128^2	30	$4.86 \cdot 10^{11}$	$\frac{1}{6}$	1.39
LR + strong backscatter	10^{-5}	128^2	30	$4.86 \cdot 10^{11}$	0	1.39
without bottom friction						
Low resolution (LR)	0	128^2	30	$4.86 \cdot 10^{11}$	-	0.93
High resolution (HR)	0	512^2	7.5	$7.59 \cdot 10^9$	-	46.7
LR + weak backscatter	0	128^2	30	$4.86 \cdot 10^{11}$	$\frac{1}{2}$	1.30
LR + moderate backscatter	0	128^2	30	$4.86 \cdot 10^{11}$	$\frac{1}{3}$	1.30
LR + strong backscatter	0	128^2	30	$4.86 \cdot 10^{11}$	$\frac{1}{4}$	1.30

Table 2.1: List of model runs used in this study. The choice of the bottom friction coefficient c_D and the biharmonic viscosity ν_B is discussed in section A.2.6. The tuning parameter for backscatter n_{diss} appears in equation ???. The total number of grid cells is denoted with N_x , the grid spacing with Δx . The computing time t_c is given in relation to the computing time of the low resolution control run with bottom friction. Please note that the computing time is only roughly estimated and strongly dependent on the computing architecture.

For the analyses in this study, we use from every model run daily in-

stantaneous values on the native model grid of 30 year long integrations. Spatial interpolation is only used in the computation of terms that involve prognostic variables from different grids (see section [A.2.1](#)). Only for the analysis of autocorrelation (section [3.6](#)) and Lagrangian trajectories (section [3.7](#)) 6-hourly data is used for a better temporal resolution. A spin-up phase of 5 years, as discussed in section [3.2](#), is disregarded from all analysis except the timeseries in Fig. [3.2](#).